Supporting Information: Towards a Theoretical Understanding of Excitonic Properties of Phthalocyanine Thin Films. I. Low-Temperature Exciton Absorption Spectra

Sanghita Sengupta,[*,†] Zheng Pei,[†] Chance Lander,[‡] Carly R. Wickizer,[‡] Yu Homma,[¶] Hadi Afshari,[§] Yuezhi Mao,[‖] Pengfei Huo,[⊥] Yu Zhang,[#] Sergei Tretiak,[*,#] Lloyd A. Bumm,[§] Madalina Furis,[*,§] and Yihan Shao[*,†]

†*Department of Chemistry & Biochemistry, University of Oklahoma, Norman, OK 73019, Department of Chemistry, Brandeis University, Waltham, MA 02453*

‡*Department of Chemistry & Biochemistry, University of Oklahoma, Norman, OK 73019*

¶*Research Center for Organic Electronics (ROEL), Yamagata University, Jonan 4-3-16, Yonezawa, Yamagata 992-8510, Japan*

§*Homer L. Dodge Department of Physics, University of Oklahoma, Norman, OK 73019*

‖*Department of Chemistry and Biochemistry, San Diego State University, San Diego, California 92182, USA*

⊥*Department of Chemistry, University of Rochester, Rochester, NY 14627*

#*Theoretical Division, Los Alamos National Laboratory, Los Alamos, NM 87545*

E-mail: ssengupta@brandeis.edu; serg@lanl.gov; madalina.furis@ou.edu; yihanshao@brandeis.edu

Contents

S1 Stereo pairs of the H_2OBPc crystal structure

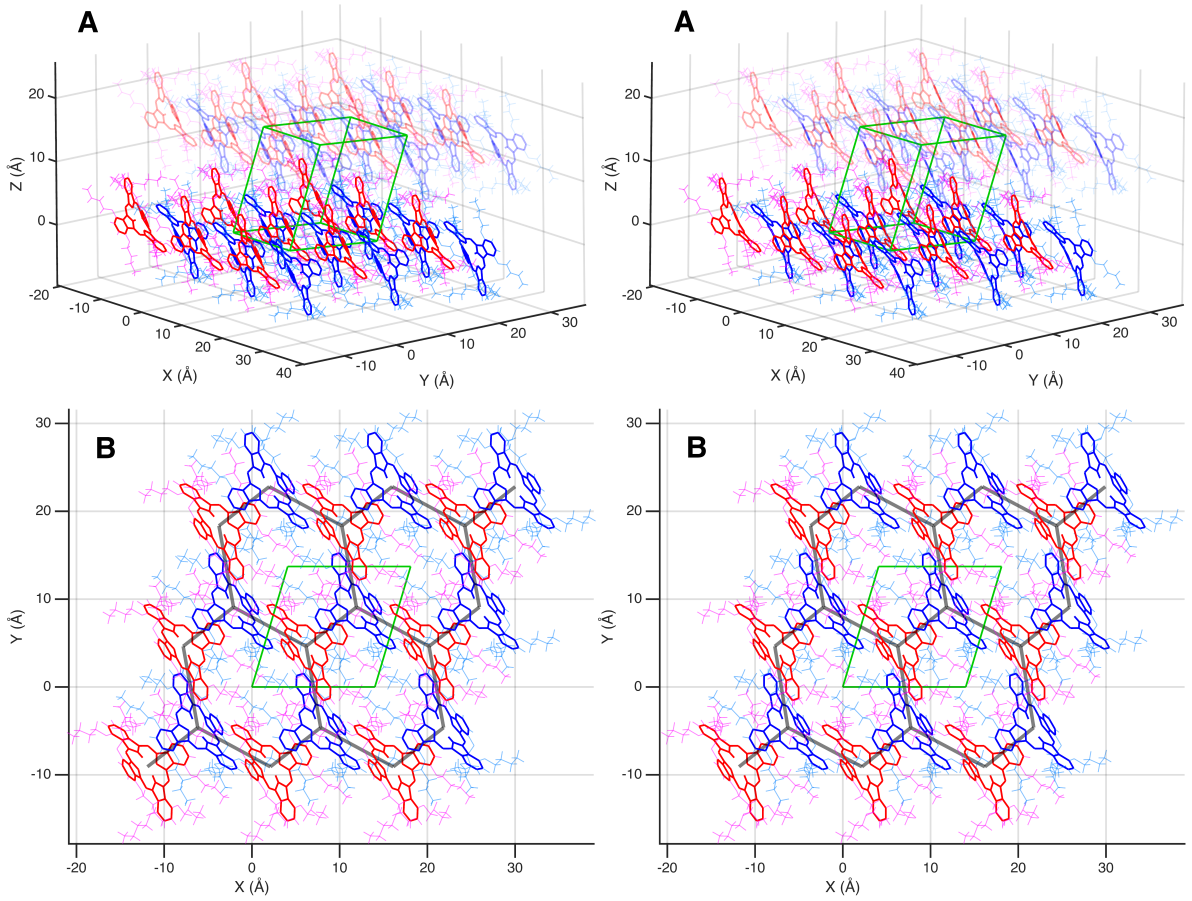

Figure S1: Eye-cross stereo pairs of the H_2OBPc crystal structure. (a) A view of a 3×3×2 tiling of unit cells. The molecules are arranged in layers of π–π interacting molecules (ab plane). The layers are stacked in the c axis interacting by the alkyl chain van der Waals interactions and longer-range π–π interactions. The unit cell from the literature is shown in green[S1] which includes the lower half of the upper layer and the upper half of the lower layer. Here the a axis is aligned with the cartesian x axis and the b axis is in the xy cartesian plane. The triclinic $P\bar{1}$ unit cell contains two molecules related by inversion symmetry. These two molecules are distinguished by color. For clarity, the Pc rings are rendered in bold red and blue. The associated alkoxy chains are magenta and cyan, respectively. The upper layer is rendered in a lighter alpha channel for clarity. (b) A view of a single layer in the ab plane tiled 3×3×1 showing the arrangement of the Pc rings in the distorted hexagonal lattice. The lower ab face of the unit cell from (a) is shown. Note that the $[1\bar{1}0]$ lattice direction (the short ab face diagonal) lies in the plane of the Pc rings. The [111] direction (long body diagonal) is perpendicular to the plane of the Pc rings. The hexagonal lattice connecting the centers of the Pc rings is shown in thick gray lines.

S2 Molecular Orbitals and Transition Densities for different functionals

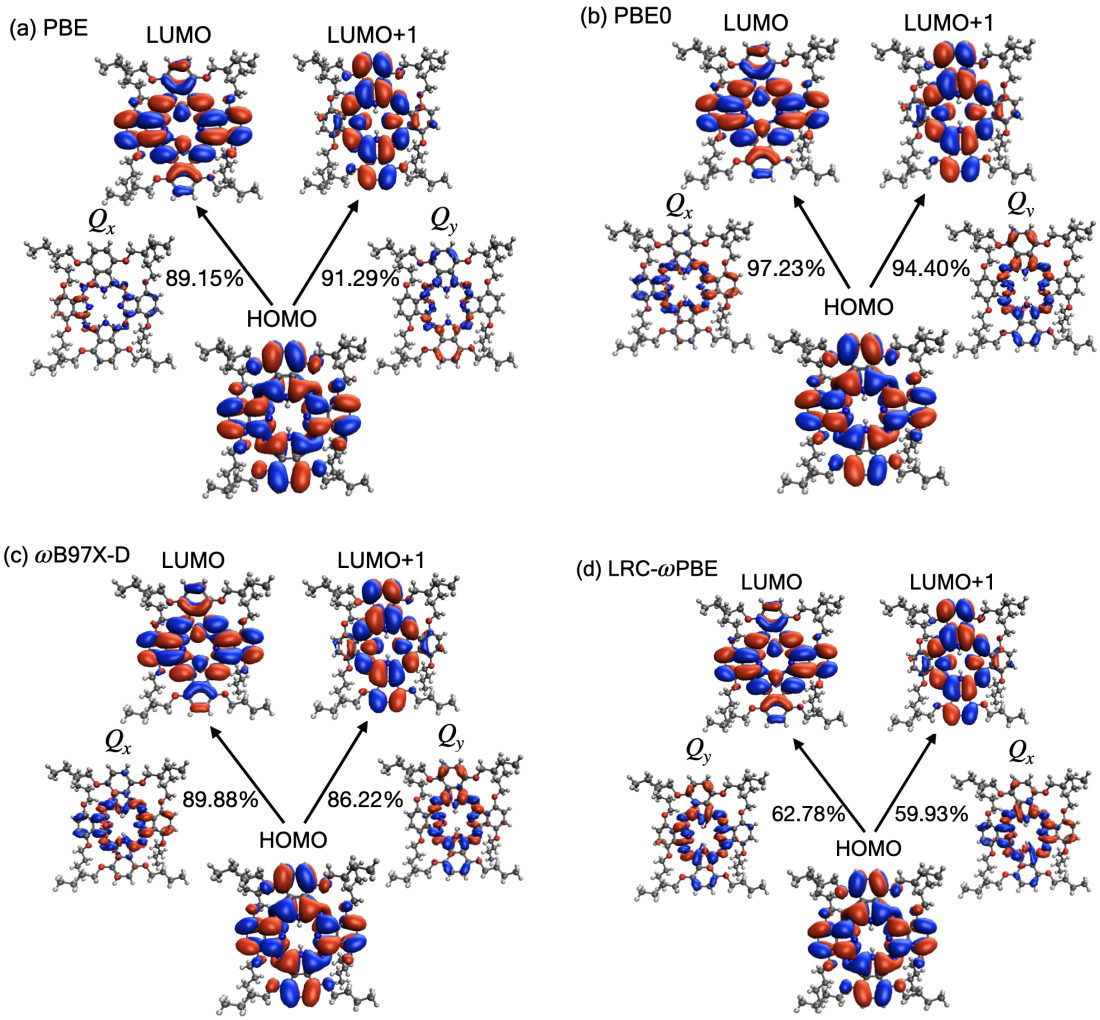

Figure S2: Frontier molecular orbitals (HOMO, LUMO, and LUMO+1) and transition densities (for Q_x and Q_y) of H_2OBPc derived from DFT and TD-DFT calculations, respectively, with four functionals and 6-31G(d,p) basis, all at the crystal monomer geometry. The percentages are the weights of the dominant excitation (HOMO→LUMO or HOMO→LUMO+1) in the Q_x and Q_y states. The isosurface values for molecular orbitals and transition densities are 0.02 and 0.001, respectively.

S3 On-site energies and Transition dipole moments across different functionals

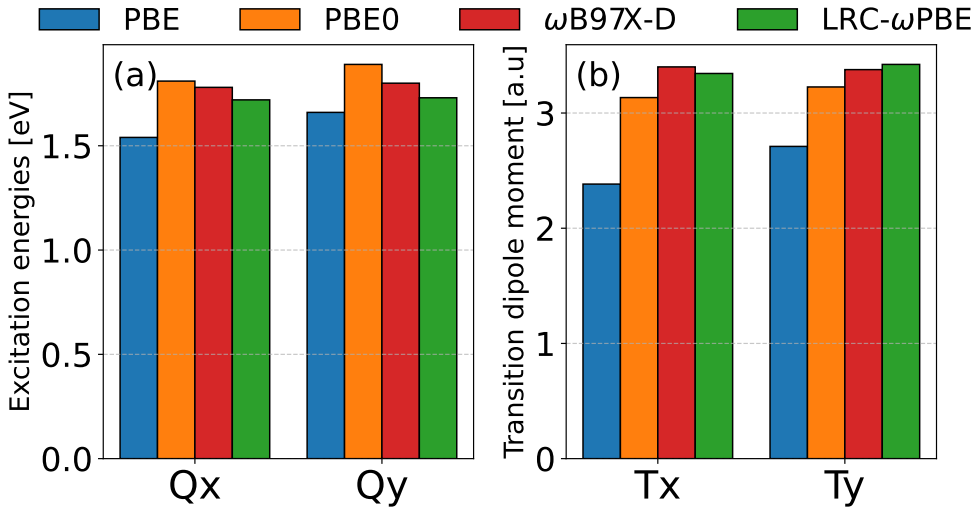

Figure S3: Functional dependences of (a) excitation energies (in eV) and (b) the norms of transition dipole moments (in a.u.) of Q_x and Q_y states of H_2OBPc obtained from TD-DFT calculations with four different functionals (PBE, PBE0, ωB97X-D, and LRC-ωPBE) and 6-31G(d,p) basis set, at the crystal monomer geometry.

Fig. S3 shows the monomer excitation energies (Q_x and Q_y) and corresponding transition dipole moments (T_x, T_y) across different functionals. Most notably, PBE calculation underestimates both excitation energies and transition dipole moments compared to the hybrid and long-range corrected functionals (PBE0, ωB97X-D, and LRC-ωPBE). This is consistent with the general expectation that a higher ratio of Hartree-Fock exact exchange increases the excitation energies.[S2] Also notable is that the difference between Q_x and Q_y energies (T_x *vs* T_y) becomes smaller with a larger ratio of long-range Hartree-Fock exchange, making Q_x and Q_y states nearly degenerate (and with similar transition dipole moments) with ωB97X-D and LRC-ωPBE functionals. This can be seen more clearly later in Fig. S7.

S4 Transition dipole moments orientations across different dimers

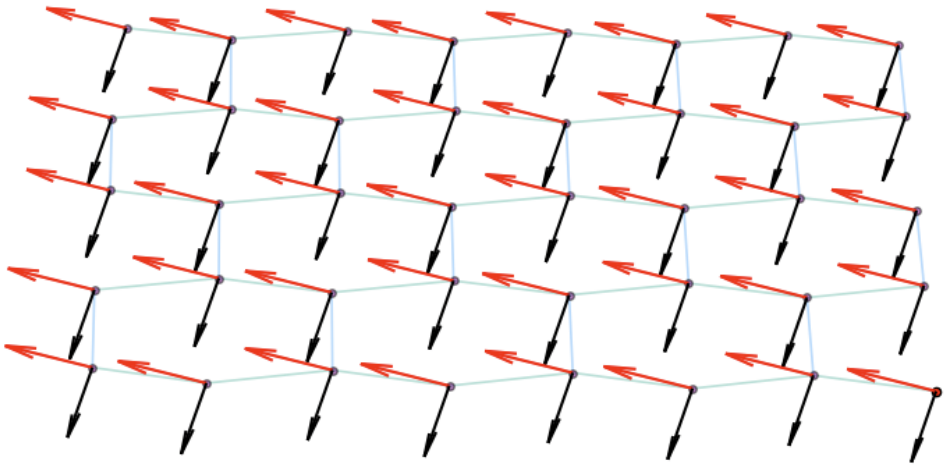

Figure S4: Orientations of transition dipole moment vectors $\mathbf{T}_x$ (black arrow) and $\mathbf{T}_y$ (red arrow) at the centers of mass for monomers in a 2D plane, corresponding to dipole-dipole interactions of dimers in 1NN (A, B, C), 2NN $(\mathcal{Z}_1,\ \mathcal{Z}_2,\ \mathcal{Z}_3)$ and 3NN $(\Omega_1\text{-}\Omega_9)$ within PBE0/6-31G(d,p) level of theory.

S5 Coulomb couplings from TD-DFT calculations at varying inter-molecular distances

Fig. S5 shows the Coulomb coupling components $J_{\mathrm{C,xx}}$, $J_{\mathrm{C,xy}}$, $J_{\mathrm{C,yx}}$ and $J_{\mathrm{C,yy}}$ (absolute values) at various dimer distances D_d computed for different functionals.

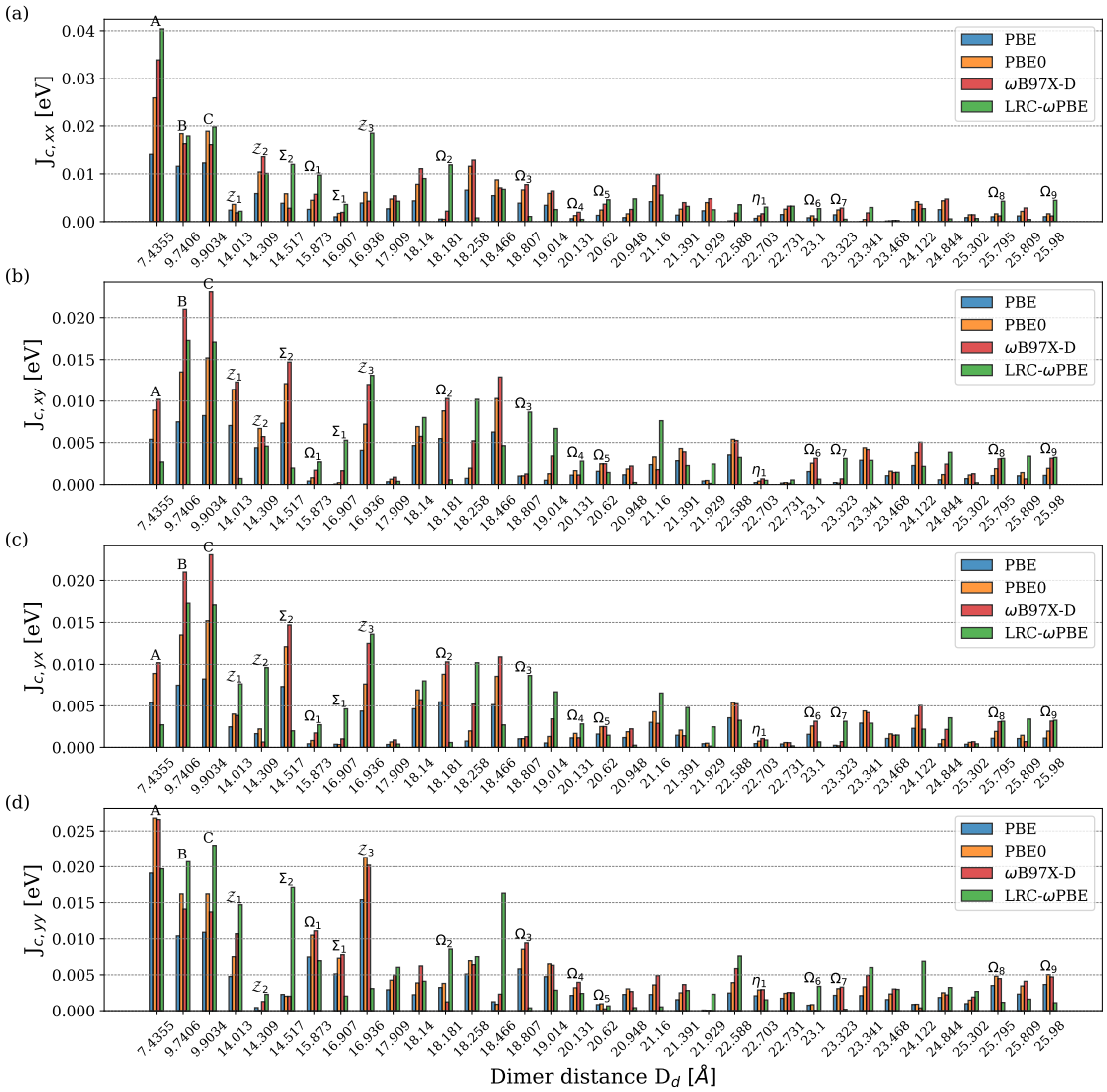

Figure S5: Coulomb couplings, $J_{\mathrm{C,xx}}$, $J_{\mathrm{C,xy}}$, $J_{\mathrm{C,yx}}$ and $J_{\mathrm{C,yy}}$ (absolute values), at various dimer distances, D_d. All values were computed using the TD-DFT transition densities of $\mathrm{Q_x}$ and $\mathrm{Q_y}$ states (Fig. S2) with four functionals and the 6-31G(d,p) basis set for dimers at the crystal geometry. The plotted values correspond to first-nearest neighbor (1NN, denoted by A, B, C), second-nearest neighbor (2NN, denoted by $\mathcal{Z}$'s) and third-nearest neighbor (3NN, denoted by Ω's) interactions, with η_1 being one of the fourth-nearest neighbor within 26 Å cutoff. Two of the shortest interlayer dimers are named as Σ_2 and Σ_1. The remaining unlabeled dimer distances correspond to other interlayer interactions.

S6 Dipole-dipole couplings from TD-DFT calculations at varying inter-molecular distances

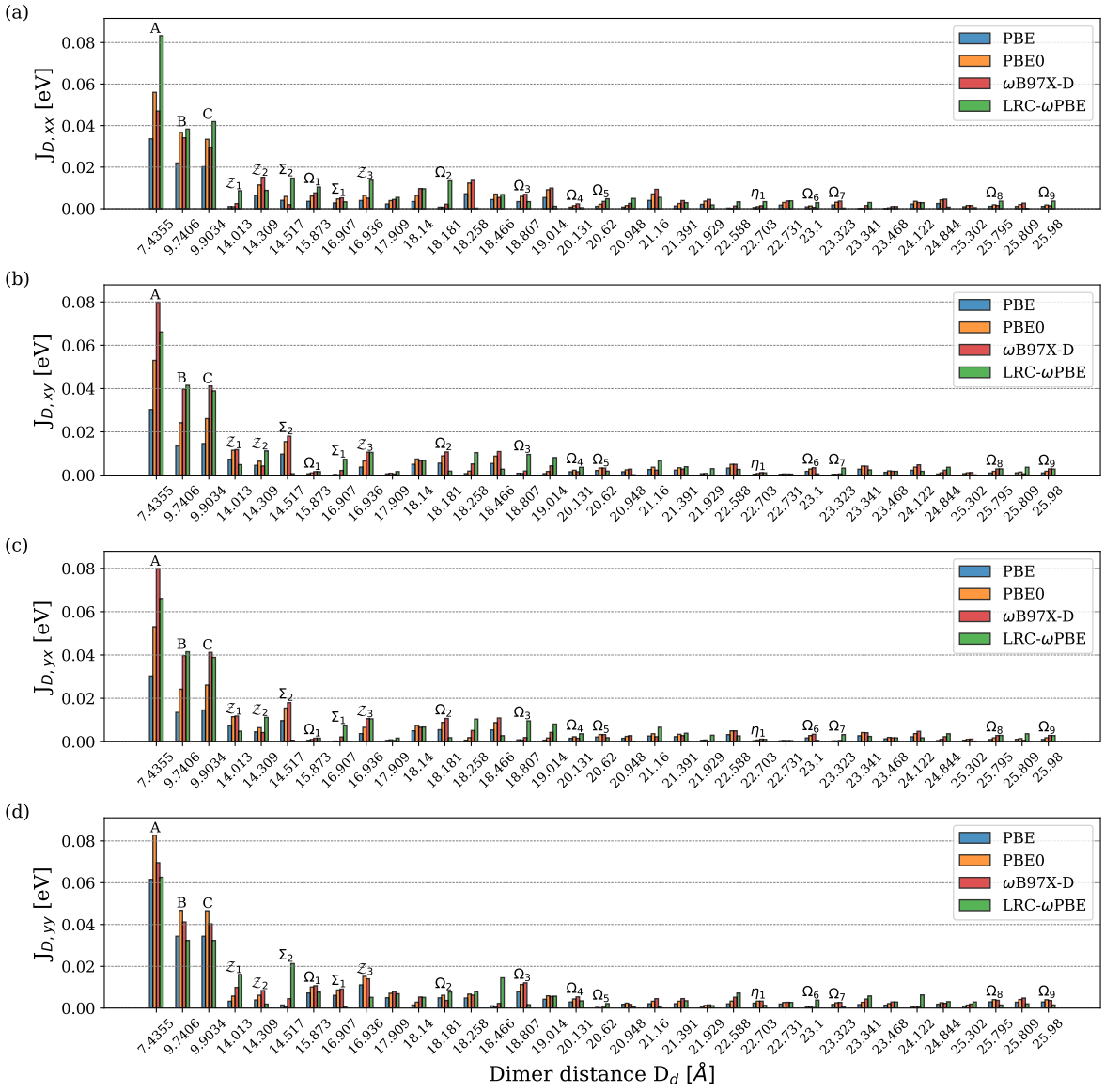

Figure S6: Dipole-dipole couplings, $J_{\mathrm{D,xx}}$, $J_{\mathrm{D,xy}}$, $J_{\mathrm{D,yx}}$ and $J_{\mathrm{D,yy}}$ (absolute values in eV), at various dimer distances, D_d. All values were computed using the TD-DFT transition dipoles for $\mathrm{Q_x}$ and $\mathrm{Q_y}$ states with four functionals and the 6-31G(d,p) basis set for dimers at the crystal geometry. The plotted values correspond to first-nearest neighbor (1NN, denoted by A, B, C), second-nearest neighbor (2NN, denoted by $\mathcal{Z}$'s) and third-nearest neighbor (3NN, denoted by Ω's) interactions, with η_1 being one of the fourth-nearest neighbor interaction within 26 Å cutoff. Two of the shortest interlayer dimers are named as Σ_2 and Σ_1. The remaining unlabeled dimer distances correspond to other interlayer interactions.

Fig. S6 shows the dipole-dipole coupling components $J_{\mathrm{D,xx}}$, $J_{\mathrm{D,xy}}$, $J_{\mathrm{D,yx}}$, and $J_{\mathrm{D,yy}}$ for all four functionals and as a function of the dimer distance (D_d). There are several distinctions between the direct Coulomb and dipole-dipole interactions: (i) the dipole-dipole couplings are in general two to three times larger; (ii) both diagonal and off-diagonal couplings are stronger in A-dimer than B- and C-dimers; and (iii) the coupling values display a more monotonic decay with the intermolecular distance, with the second-nearest and interlayer neighbors coupled much more weakly than the nearest neighbors. Therefore, while conceptually simpler to interpret, the *dipole-dipole couplings overestimate the exciton coupling and should be used with caution*.

S7 Simulated exciton absorption for monomer and first-nearest neighbor dimers using direct Coulomb coupling and dipole-dipole interactions

Figs. S7(a-d) and S8(a-d) show the absorption spectra for monomer and the respective dimer geometries A, B, and C using the direct Coulomb couplings and dipole-dipole interactions across all the functionals.

Several qualitative observations are made in conjunction with interaction magnitudes given in Figs. S3 and S5. (i) *Monomer Spectra and Functional Dependence:* Relative to ωB97X-D and LRC-ωPBE, a more significant splitting in monomer spectra is observed with PBE and PBE0, which correspond to the aforementioned larger differences in Q_x and Q_y-state energy values with these functionals. Theoretically, the Q_x-Q_y energy splitting can be traced to the lifting of LUMO/LUMO+1 degeneracy, when the molecular point group symmetry is reduced from D_{4h} to D_{2h} upon the introduction of two hydrogen atoms (next to two nitrogen atoms) in the macrocycle ring. Clearly, the four functionals display different sensitivity to such symmetry breaking. Amongst, the TD-PBE0 calculated Q-band splitting of $\sim$26.4 nm closely matches the experimental value of $\sim$21 nm.[S3–S6] (ii) *Coulomb vs dipole-dipole coupling:* As mentioned earlier, the Coulomb interaction is smaller in magnitude than dipole-dipole coupling. This is well reflected in the dimer absorption spectra, where the employment of dipole-dipole coupling led to more pronounced splitting and systematic shifts in the absorption peak.

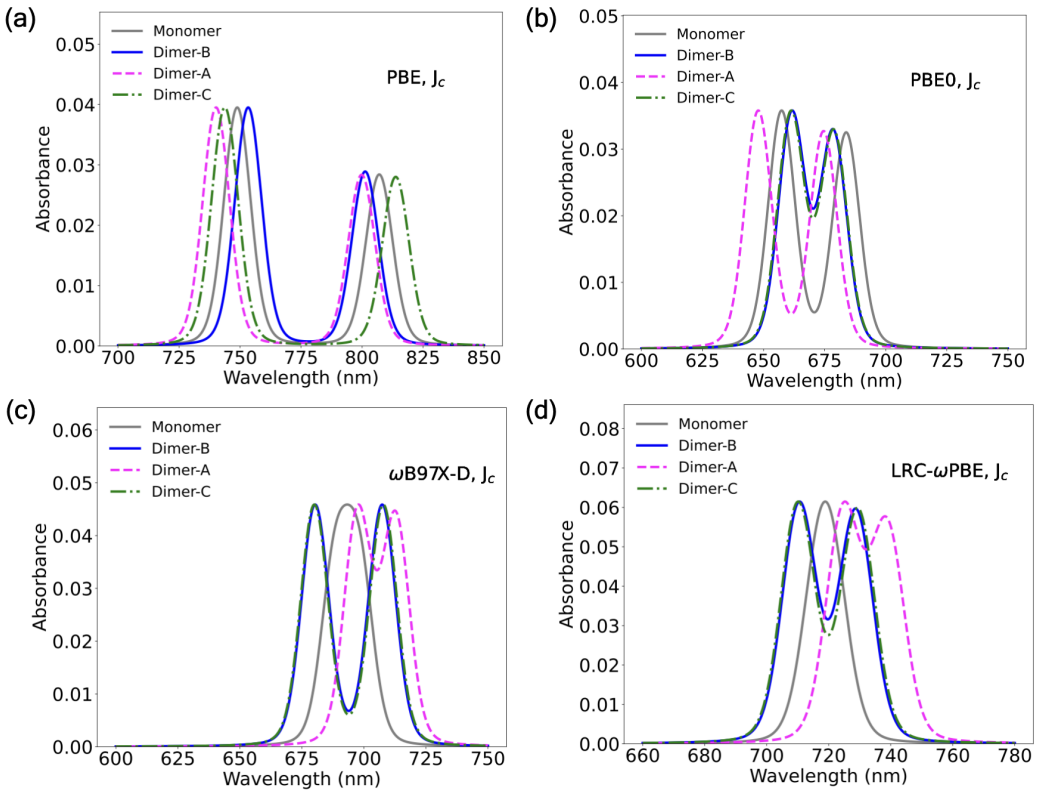

Figure S7: Predicted exciton absorption spectra for monomer and dimers A, B, and C with Coulomb couplings from four different functionals and 6-31G(d,p) basis set at the crystal geometry. Voigt profile broadening is used with Gaussian broadening $\sigma = 5$ nm and Lorentzian broadening $\gamma = 2.25$ nm.

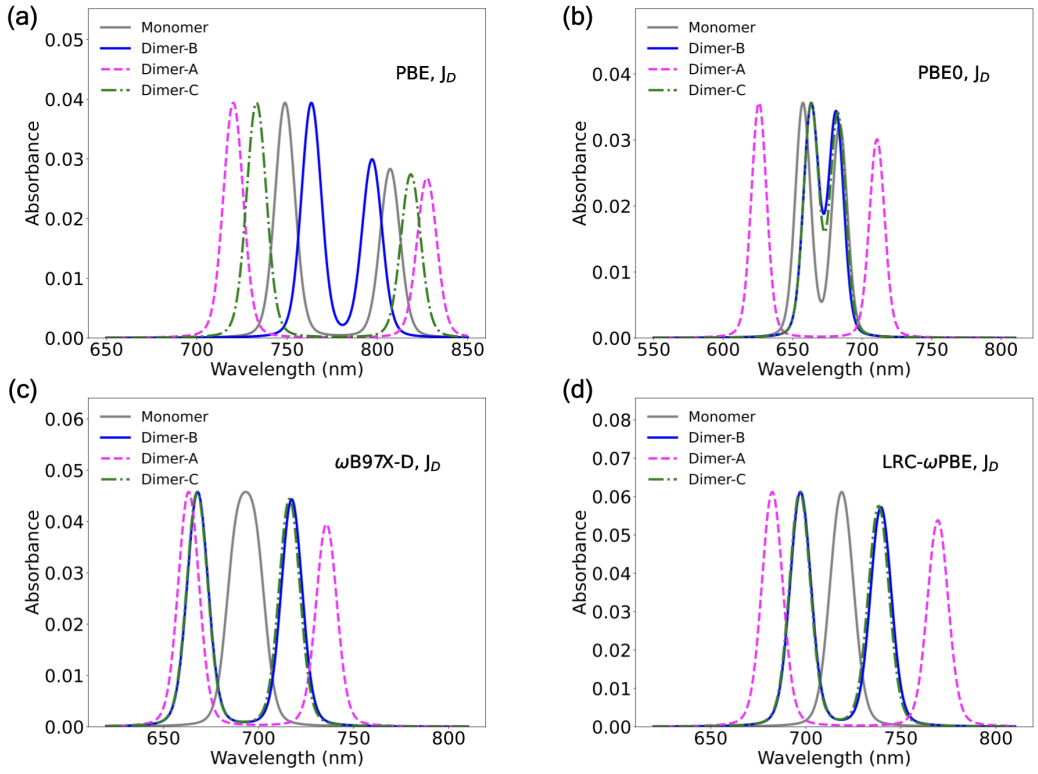

Figure S8: Predicted exciton absorption spectra for monomer and dimers A, B, and C with dipole-dipole couplings from four different functionals and 6-31G(d,p) basis set at the crystal geometry. Voigt profile broadening is used with Gaussian broadening $\sigma = 5$ nm and Lorentzian broadening $\gamma = 2.25$ nm.

S8 Exciton absorption spectra for molecular aggregates in 1D for various functionals

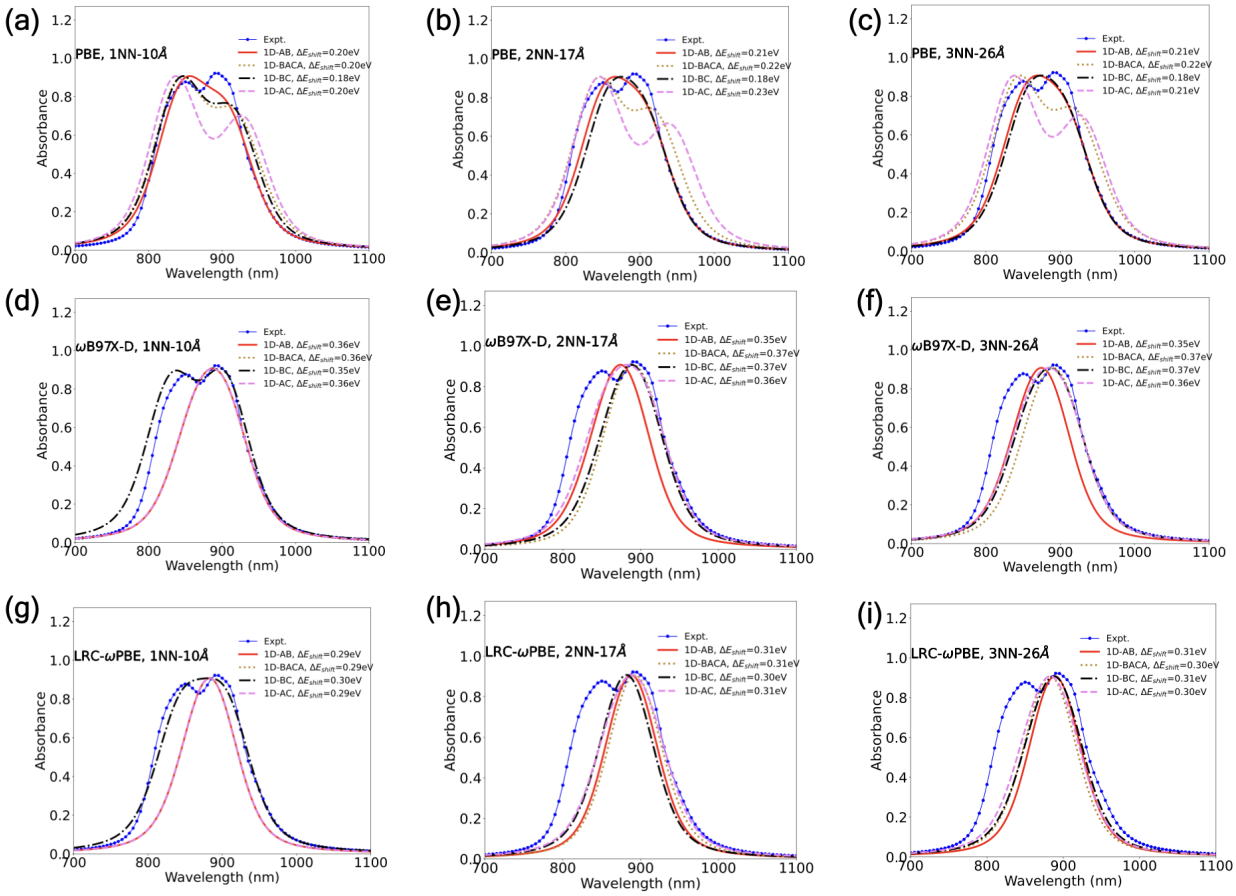

Figure S9: Predicted exciton normalized absorption spectra of various 1D models of 600 H_2OBPc molecules using *Coulomb couplings* (J_C) at 10, 17 or 26 Å distance cutoffs from TD-DFT calculations with three functionals and the 6-31G(d,p) basis set. (a,d,g) Only nearest neighbor couplings (A, B, C) are included within 10 Å distance cutoff. (b,e,h) When the cutoff is increased to 17 Å, all second nearest neighbors ($\mathcal{Z}_1$, $\mathcal{Z}_2$, $\mathcal{Z}_3$) and third nearest neighbor (Ω_1 only in the case of 1D-BACA) are also added to the Frenkel Hamiltonian. (c,f,i) Cutoff 26 Å, all third nearest neighbors. ΔE_{shift} corresponds to an additional shift (in nm) to better match the two experimental peaks. Gaussian broadening of $\sigma = 25$ nm and Lorentzian broadenings of $\gamma = 20$ nm are used.

S9 Exciton absorption spectra for molecular aggregates across different dimensions using direct Coulomb coupling for various functionals

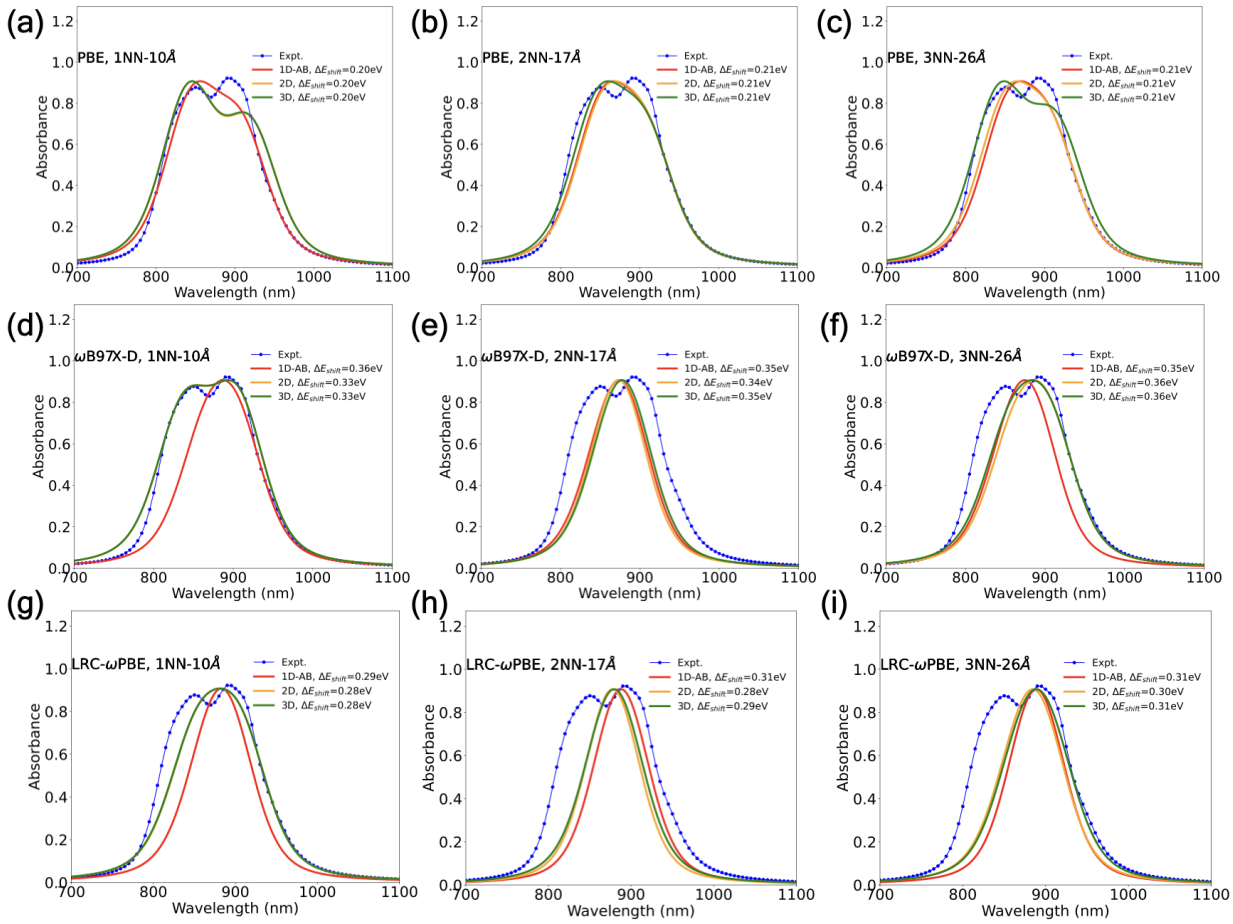

Figure S10: Predicted exciton normalized absorption spectra of 600 H_2OBPc molecules from 1D-AB, 2D, and 3D models using *Coulomb coupling* (J_C) from TD-DFT calculations with (a–c) PBE, (d–f) ωB97X-D, and (g–i) LRC-ωPBE functionals using 6-31G(d,p) basis. Gaussian broadening of $\sigma = 25$ nm and Lorentzian broadening of $\gamma = 20$ nm are used.

S10 Comparison of exciton absorption spectra for molecular aggregates for 1D-BC and 2D models using direct Coulomb coupling for PBE0

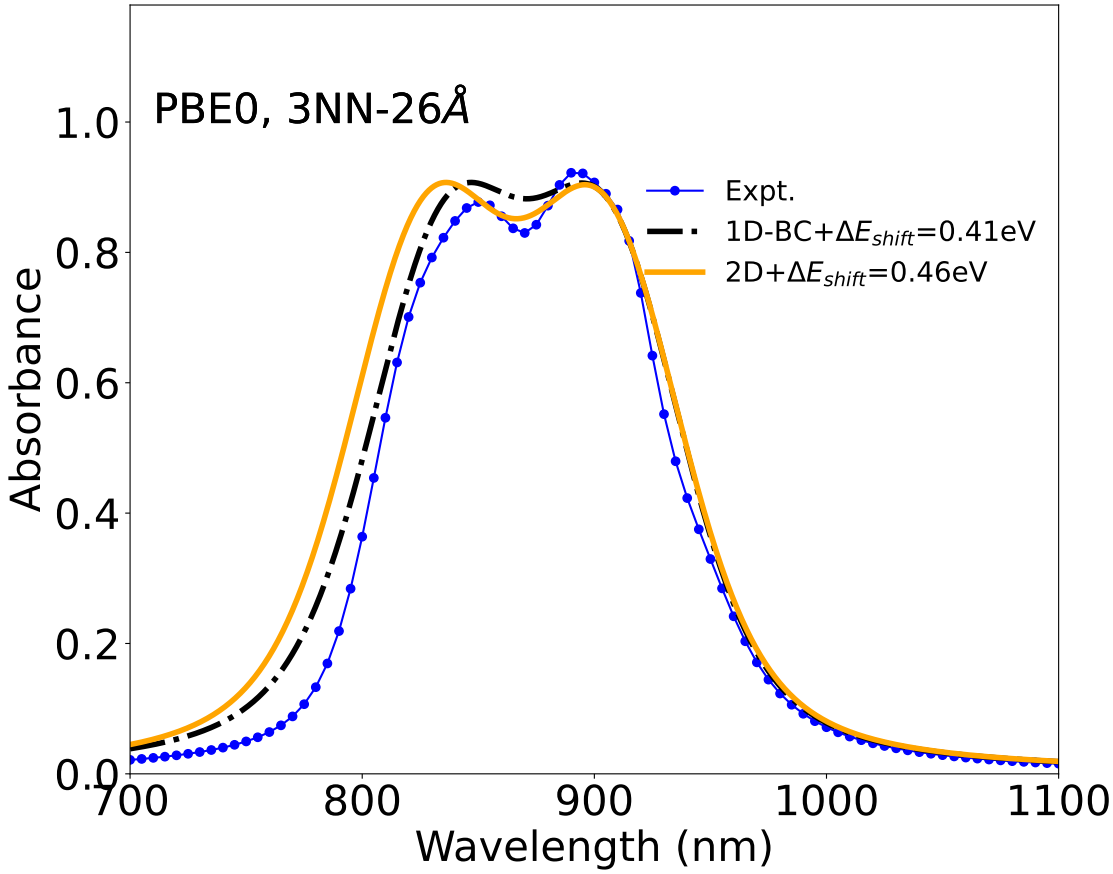

Figure S11: Comparison of normalized absorption spectra obtained with 1D-BC and 2D models both at 26 Å cutoff using PBE0/6-31G(d,p). A Gaussian broadening of $\sigma = 25$ nm and Lorentzian broadenings of $\gamma = 20$ nm are used. At the same level of parameters, the 2D model shows a slightly larger broadening compared to the 1D-BC. While the second peak overlaps for both the models, the first peak for the 2D model is at a lower wavelength compared to the 1D-BC.

S11 Exciton absorption spectra for molecular aggregates across different dimensions using dipole-dipole couplings for various functionals

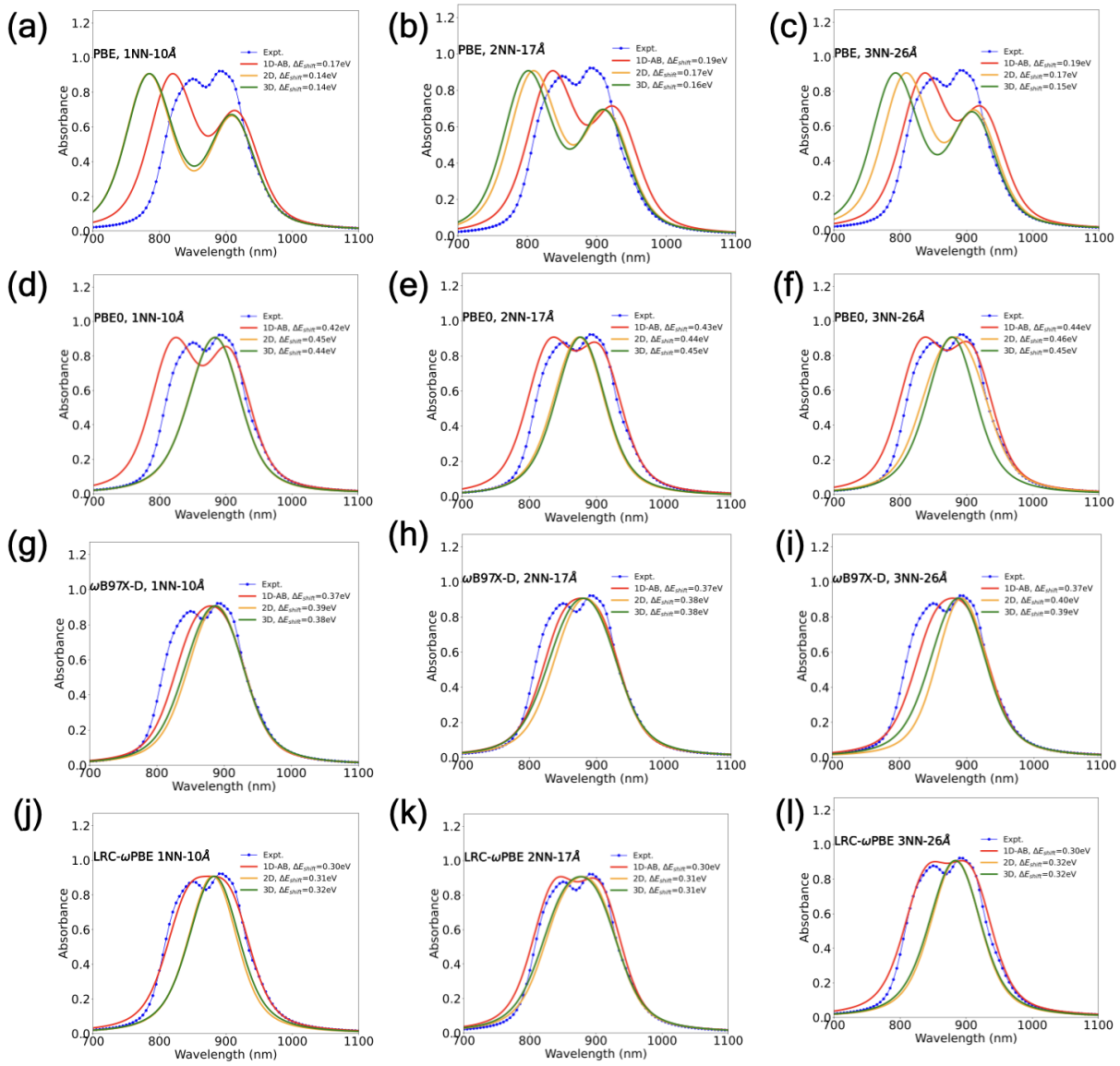

Figure S12: Predicted exciton normalized absorption spectra of 600 H_2OBPc molecules with 1D-AB, 2D, and 3D models using *dipole-dipole couplings* (J_D) from TD-DFT calculations. Voigt profile with Gaussian broadening $\sigma = 25$ nm and Lorentzian Broadening with $\gamma = 20$ nm is used for all functionals with 6-31G(d,p) basis.

S12 Convergence of simulated absorption spectra across different dimensionalities and various distance cut-offs

In this section we provide the variation of the exciton Coulomb couplings for various intermolecular distances which go beyond the 26 Å cutoff (shown in the main text).

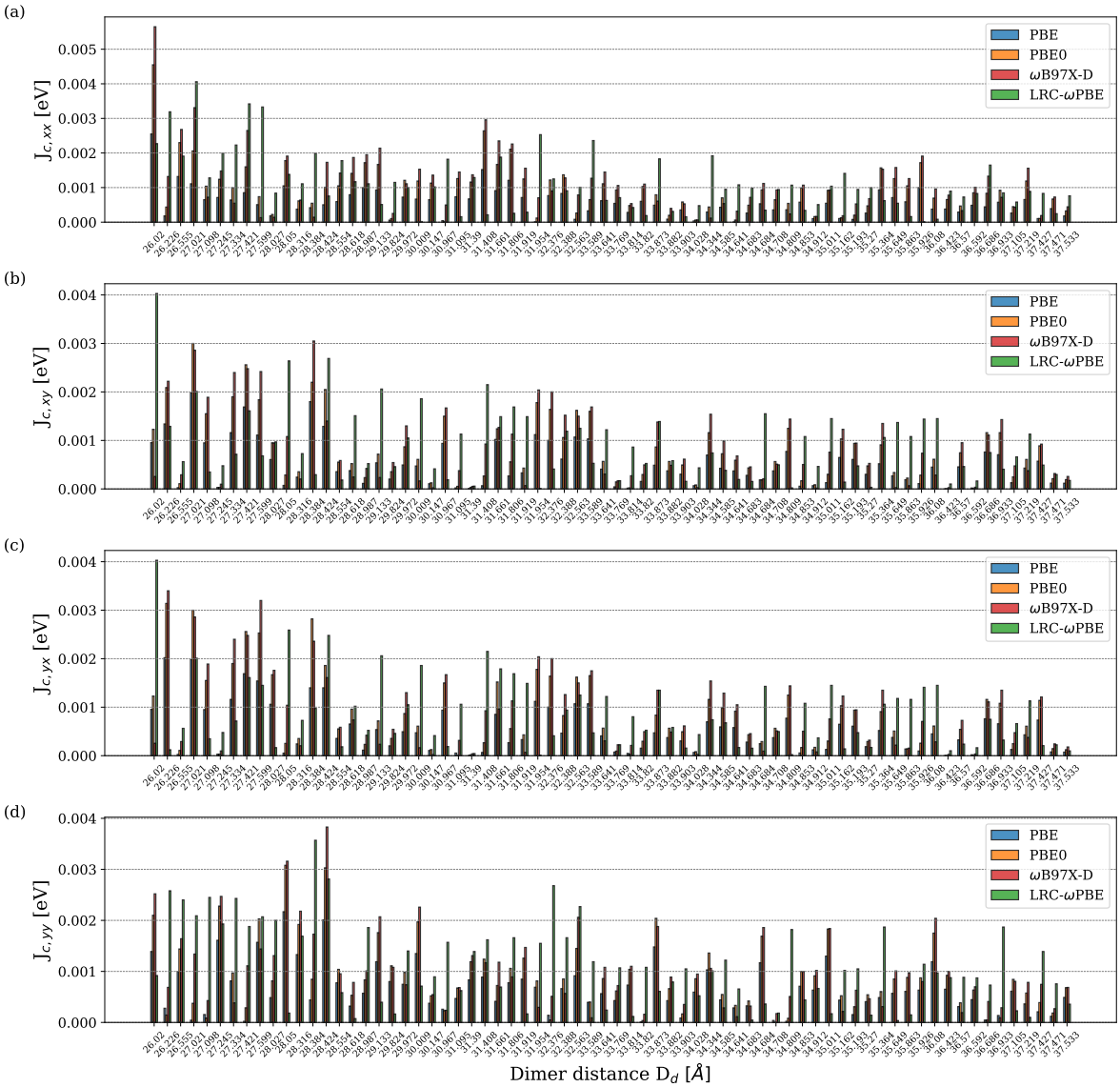

Figure S13: Coulomb couplings, $J_{\mathrm{C,xx}}$, $J_{\mathrm{C,xy}}$, $J_{\mathrm{C,yx}}$, and $J_{\mathrm{C,yy}}$ (absolute values), at various dimer distances, $\mathrm{D}_d \geq 26$ Å. All values are computed using the TD-DFT transition densities of Q_x and Q_y states (Fig. S2) with four functionals and the 6-31G(d,p) basis set for dimers at the crystal geometry. For dimer distances smaller than 26 Å, see the main text.

This section presents the convergence of the stimulated absorption spectra for a molecular aggregate of 600∼1800 molecules for PBE0/6-31G(d,p) across different dimensionalities and various distance cutoffs such as $r_{\text{cut}} = 10, 17$, and 26 Å. The 3D multi-layer results (2-6 layers) are shown in panels (j–l) of Fig. S14.

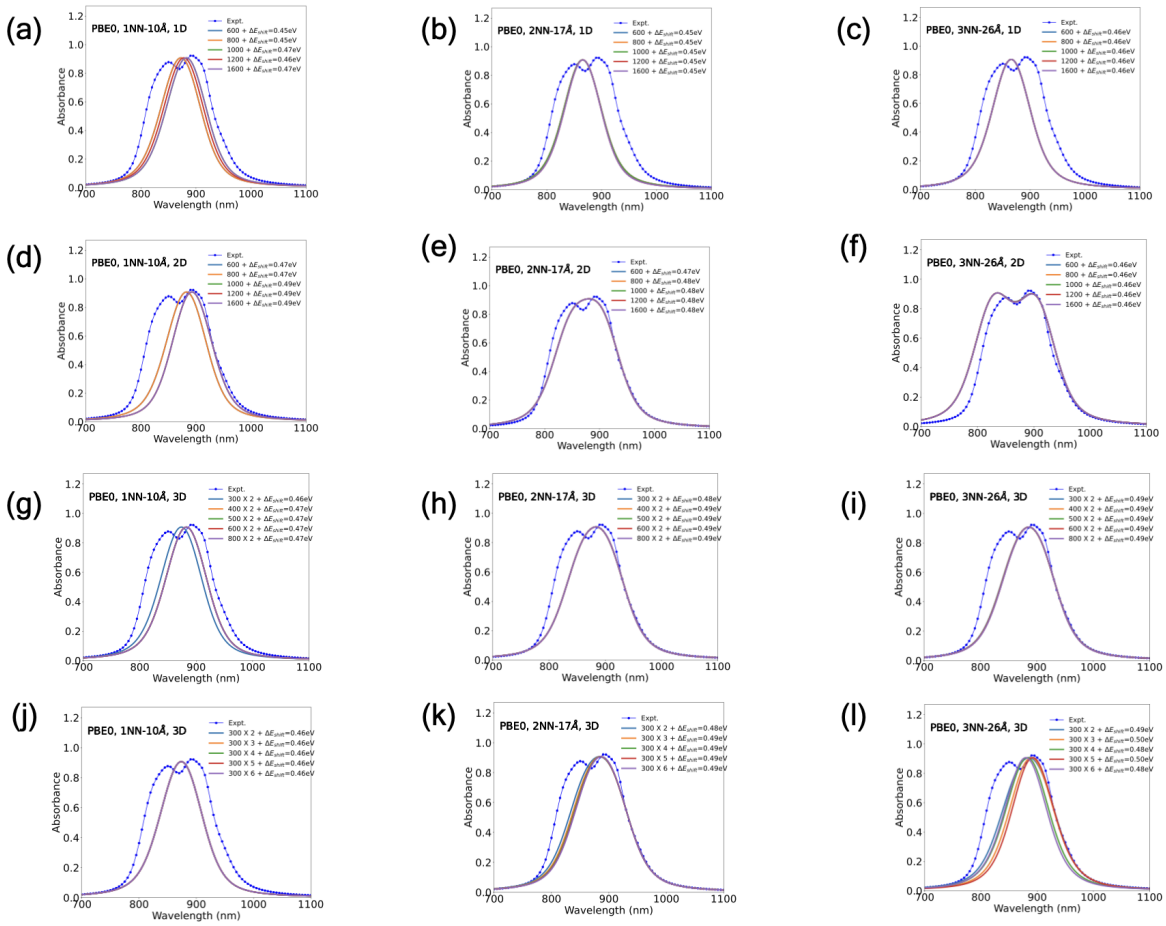

Figure S14: Predicted exciton normalized absorption spectra of 600–1800 H_2OBPc molecules using (a–c) 1D-AB, (d–f) 2D, (g–i) two-layer 3D, and (j–l) multi-layer (2–6) 3D models with multi-layers using *Coulomb couplings* (J_C) from PBE0/6-31G(d,p) TD-DFT calculations at three distance cutoffs (10, 17, and 26 Å). For the 2D systems, as the number of molecules increases from 600 to 1600, the construction is such that additional molecules are systematically added along the x-direction. Voigt profile with Gaussian broadening $\sigma = 25$ nm and Lorentzian Broadening with $\gamma = 20$ nm is used.

S13 Polarization-dependent absorption spectra

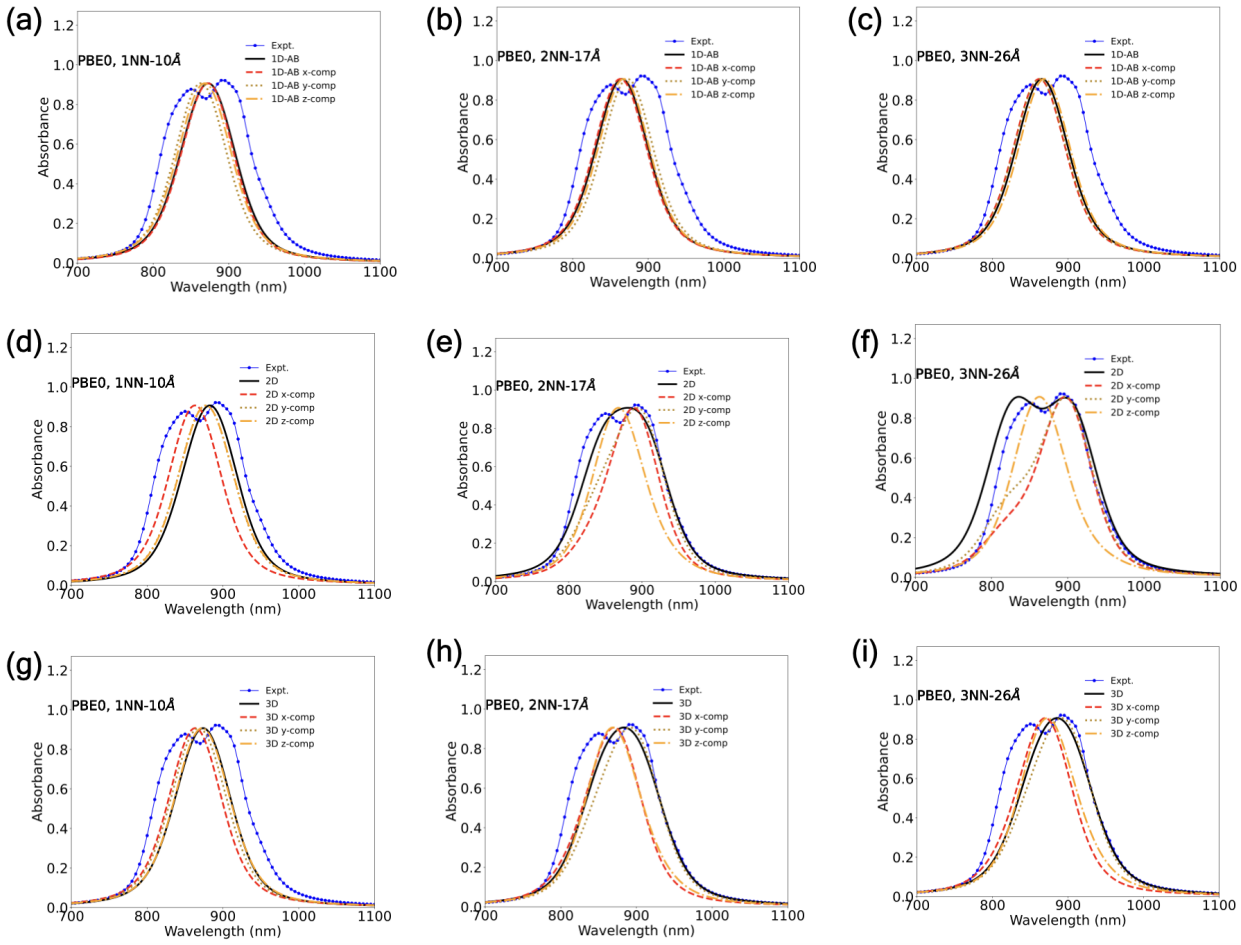

Figure S15: Predicted exciton normalized absorption spectra of 600 H_2OBPc molecules using 1D-AB, 2D, and 3D models using *Coulomb coupling* (J_C) from TD-DFT calculations (PBE0/6-31G(d,p) level of theory) with different components of transition dipole moment vector $\vec{T}$, viz. x, y or z with Gaussian broadening $\sigma = 25$ nm and Lorentzian broadening $\gamma = 20$ nm.

S14 Basis Dependence

Tables S1 and S2 show the basis set dependence of the on-site energies (Q), transition dipole moments (T) and Coulomb couplings (J_{C}) of the PBE0 functional. The 6-31G(d,p) basis set used in the main text is benchmarked with the following basis sets: 6-31+G(d,p),[S7] def2-SVPD,[S8,S9] aug-cc-pVDZ,[S10,S11] and 6-311++G(d,p).[S12]

Table S1: Onsite energies (eV), onsite energy gap (eV), and first and second excited state transition dipole moments (T_{x} and T_{y}) for the H_2OBPc monomer with varying basis sets. All calculations are performed using the PBE0 functional. Calculations in the main text were performed using the 6-31G(d,p) basis set.

Basis	Q_{x}	Q_{y}	$\lvert Q_{\mathrm{y}} - Q_{\mathrm{x}}\rvert$	$T_{\mathrm{x},x}$	$T_{\mathrm{x},y}$	$T_{\mathrm{x},z}$	$T_{\mathrm{y},x}$	$T_{\mathrm{y},y}$	$T_{\mathrm{y},z}$
6-31G(d,p)	1.813	1.886	0.073	1.749	0.228	-2.588	1.468	-2.759	0.794
6-31+G(d,p)	1.786	1.862	0.076	1.754	0.256	-2.620	1.508	-2.796	0.776
def2-SVPD	1.779	1.854	0.075	1.765	0.229	-2.606	1.495	-2.801	0.797
aug-cc-pVDZ	1.774	1.847	0.074	1.758	0.241	-2.612	1.516	-2.817	0.789
6-311++G(d,p)	1.781	1.855	0.074	1.760	0.249	-2.622	1.510	-2.808	0.784

Table S2: Coulomb couplings (J_{C} in meV) for dimers A, B, and C with varying basis sets. All calculations are performed using the PBE0 functional. Calculations in the main text were performed using the 6-31G(d,p) basis set.

Dimer	Basis	$J_{\mathrm{C,xx}}$	$J_{\mathrm{C,xy}}$	$J_{\mathrm{C,yx}}$	$J_{\mathrm{C,yy}}$
A	6-31G(d,p)	-25.915	-8.907	-8.907	-26.771
	6-31+G(d,p)	-26.030	-9.288	-9.288	-27.531
	def2-SVPD	-26.104	-9.296	-9.296	-27.584
	aug-cc-pVDZ	-26.206	-9.288	-9.288	-27.679
	6-311++G(d,p)	-26.189	-9.384	-9.384	-27.695
B	6-31G(d,p)	-18.400	13.506	13.506	16.188
	6-31+G(d,p)	-18.975	13.563	13.563	17.380
	def2-SVPD	-18.701	13.736	13.736	17.116
	aug-cc-pVDZ	-18.707	13.545	13.545	17.153
	6-311++G(d,p)	-18.930	13.675	13.675	17.548
C	6-31G(d,p)	-18.856	15.161	15.161	16.225
	6-31+G(d,p)	-19.426	15.201	15.201	17.372
	def2-SVPD	-19.016	15.383	15.383	17.087
	aug-cc-pVDZ	-19.022	15.198	15.198	17.180
	6-311++G(d,p)	-19.323	15.329	15.329	17.602

S15 Broadening dependence of absorption spectra across all dimensions

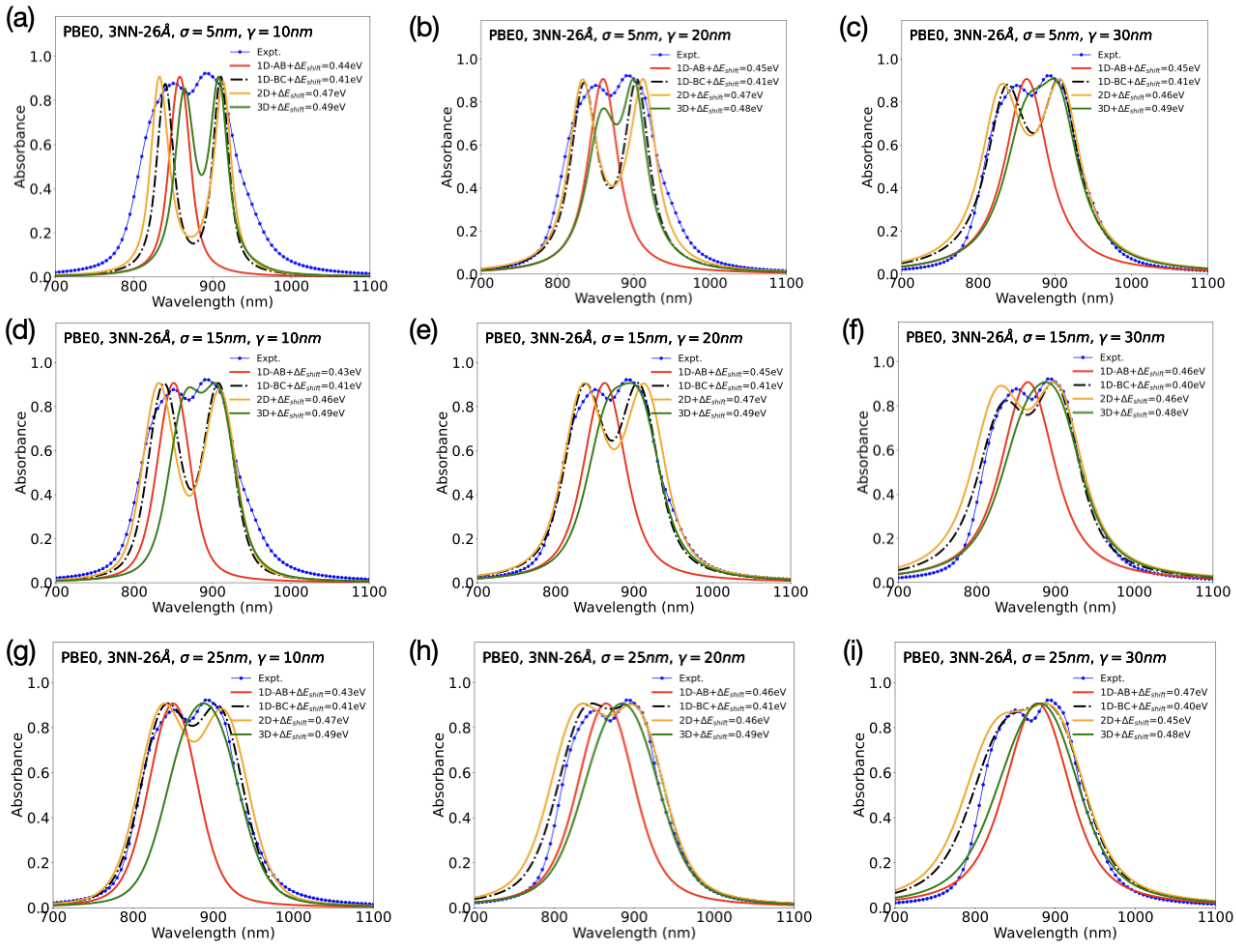

Figure S16: Predicted exciton normalized absorption spectra of 600 H_2OBPc molecules using 1D-AB, 1D-BC, 2D, and 3D models using *Coulomb coupling* (J_C) from PBE0/6-31G(d,p) TD-DFT calculations with 26 Å distance cutoff for dimer interactions and different values of Gaussian σ and Lorentzian γ broadenings.

References

(S1) Gao, Y.; Chen, Y.; Li, R.; Bian, Y.; Li, X.; Jiang, J. Nonperipherally Octa(butyloxy)-Substituted Phthalocyanine Derivatives with Good Crystallinity: Effects of Metal–Ligand Coordination on the Molecular Structure, Internal Structure, and Dimensions of Self-Assembled Nanostructures. *Chem. Eur. J.* **2009**, *15*, 13241–13252.

(S2) Shao, Y.; Mei, Y.; Sundholm, D.; Kaila, V. R. I. Benchmarking the Performance of Time-Dependent Density Functional Theory Methods on Biochromophores. *J. Chem. Theory Comput.* **2020**, *16*, 587–600.

(S3) Liang, L.; Burrill, K.; Furis, M. I. Transition Dipole Moments of One-Dimensional Excitons in Soluble Phthalocyanine Thin Films. *J. Phys. Chem. C* **2021**, *125*, 27966–27974.

(S4) Rawat, N.; Pan, Z.; Manning, L. W.; Lamarche, C. J.; Cour, I.; Headrick, R. L.; Waterman, R.; Woll, A. R.; Furis, M. I. Macroscopic Molecular Ordering and Exciton Delocalization in Crystalline Phthalocyanine Thin Films. *J. Phys. Chem. Lett.* **2015**, *6*, 1834–1840, PMID: 26263257.

(S5) Baeten, Y.; Fron, E.; Ruzié, C.; Geerts, Y. H.; Van Der Auweraer, M. Investigation of the Q–Q Equilibrium in a Metal-Free Phthalocyanine. *ChemPhysChem* **2015**, *16*, 3992–3996.

(S6) Murray, C.; Dozova, N.; McCaffrey, J. G.; Shafizadeh, N.; Chin, W.; Broquier, M.; Crépin, C. Visible luminescence spectroscopy of free-base and zinc phthalocyanines isolated in cryogenic matrices. *Phys. Chem. Chem. Phys.* **2011**, *13*, 17543–17554.

(S7) Clark, T.; Chandrasekhar, J.; Spitznagel, G. W.; Schleyer, P. V. R. Efficient diffuse function-augmented basis sets for anion calculations. III. The 3-21+G basis set for first-row elements, Li–F. *J. Comput. Chem.* **1983**, *4*, 294–301.

(S8) Weigend, F.; Ahlrichs, R. Balanced basis sets of split valence, triple zeta valence and quadruple zeta valence quality for H to Rn: Design and assessment of accuracy. *Phys. Chem. Chem. Phys.* **2005**, *7*, 3297.

(S9) Rappoport, D.; Furche, F. Property-optimized Gaussian basis sets for molecular response calculations. *J. Chem. Phys.* **2010**, *133*, 134105.

(S10) Dunning, T. H. Gaussian basis sets for use in correlated molecular calculations. I. The atoms boron through neon and hydrogen. *J. Chem. Phys.* **1989**, *90*, 1007–1023.

(S11) Kendall, R. A.; Dunning, T. H.; Harrison, R. J. Electron affinities of the first-row atoms revisited. Systematic basis sets and wave functions. *J. Chem. Phys.* **1992**, *96*, 6796–6806.

(S12) Krishnan, R.; Binkley, J. S.; Seeger, R.; Pople, J. A. Self-consistent molecular orbital methods. XX. A basis set for correlated wave functions. *J. Chem. Phys.* **1980**, *72*, 650–654.